Probing QCD at the Highest Q^2 Deep Inelastic Scattering

James Ferrando

University of Oxford, Particle Physics, Denys Wilkinson Building, Keble Road, Oxford, United Kingdom OX1 3RH.

arXiv:0910.3379v1 [hep-ex] 18 Oct 2009

Abstract

Recent results from the HERA ep collider are reviewed in these proceedings. The results are from measurements that probe QCD at high-energy scales, as defined by Q^2, the four-momentum-transfer squared of the collisions. These cross-section measurements provide information about the parton distribution functions (PDFs) of the proton and can be used to constrain global fits of these PDFs. Recent measurements of the strong coupling α_S and jet substructure from HERA at similar energy scales are also reviewed.

1. Introduction

The Hadron-Elektron Ringanlage (HERA) was the first and, so far, only electron-proton collider in the world. At HERA, protons were collided with electrons (e^+ or e^-) at the interaction region of the H1 and ZEUS detectors. The collider was operational from 1992 until 2007. The proton beam energy was 820 GeV from 1994–1997 and then 920 GeV until 2007. In the final months of HERA running, proton energies of 460 GeV and 575 GeV were used for the purposes of measuring the longitudinal structure function F_L. The electron beam energy was 27.5 GeV throughout the whole of HERA running.

Between 2000 and 2003, HERA underwent a luminosity upgrade and was also modified to enable production of longitudinally-polarised electron beams. The data taken before (after) this upgrade are referred to as HERA-I (HERA-II) data.

HERA was the location *par excellence* for the measurement of proton structure. The HERA experiments extended the kinematic reach of Deep Inelastic Scattering (DIS) experiments by several orders of magnitude in photon virtuality, Q^2, and Bjorken-x. In addition, the use of a proton beam rather than a nuclear target meant that no nuclear corrections were needed for use in extracting the parton distribution functions (PDFs) of the proton. The use of both e^+ and e^- beams means that electroweak effects can be exploited for sensitivity to cross-section contributions from different quarks.

The electron-proton collision environment is also ideal for jet physics. Jets were copiously produced at HERA and underlying event activity is much less significant in electron-proton collisions than in hadron-hadron collisions. Jet production cross sections are sensitive to the strong coupling, α_S, and the gluon PDF. The large quantity of jets produced means that the substructure of jets can also be studied.

2. Structure Functions and PDFs

The double-differential cross section for neutral current (NC) DIS with unpolarised $e^\pm p$ beams can be written [1] in terms of Q^2, x and the electron inelasticity, y, as:

$$\frac{\mathrm{d}^2\sigma^{e^\pm p}_{NC}}{\mathrm{d}x\mathrm{d}Q^2} = \frac{2\pi\alpha^2 Y_+}{xQ^4}[F_2(x,Q^2) \mp \frac{Y_-}{Y_+}xF_3(x,Q^2) - \frac{y^2}{Y_+}F_L(x,Q^2)]\,(1+\delta_r) \quad (1)$$

where F_2, xF_3 and F_L are the proton structure functions, δ_r is an electroweak radiative correction, and $Y_\pm = 1 \pm (1-y)^2$.

At leading order in Quantum Chromodynamics (QCD), $F_2 \propto \sum_i \{xq_i(x,Q^2) + x\bar{q}_i(x,Q^2)\}$ where q_i ($\bar{q}_i$) are the parton distribution functions for the (anti)quarks. This F_2 term dominates the cross section over the majority of the kinematic region. The parity violating structure function xF_3 is proportional to $\sum_i \{xq_i(x,Q^2) - x\bar{q}_i(x,Q^2)\}$, i.e. the valence quarks. This xF_3 term is significant only at high values of Q^2. At leading order in QCD the longitudinal structure function F_L is zero. However, once higher order terms are taken into account, it can be seen that F_L has a value proportional to the gluon PDF and the strong coupling. The F_L term becomes significant at low values of Q^2 and high values of y.

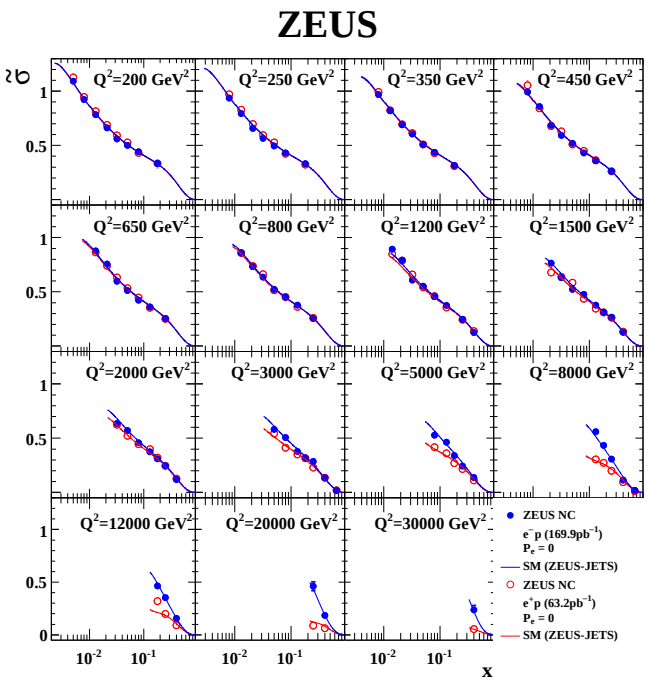

Fig. 1. The reduced cross sections for NC DIS in $e^\pm$ collisions.

2.1. Measurements of F_2 and xF_3

If one divides the double-differential cross section for NC by the "propagator" term $\frac{2\pi\alpha^2 Y_+}{xQ^4}$ and the electroweak radiative correction then one obtains $\tilde{\sigma}$, the reduced cross section at Born level:

©2009 by Universal Academy Press, Inc.

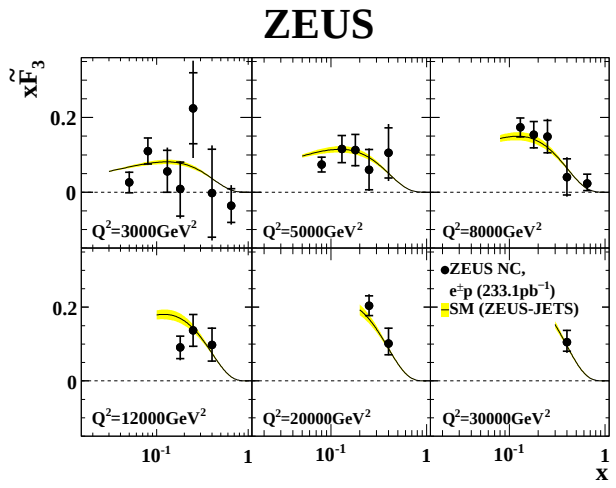

Fig. 2. The parity violating structure function xF_3 as measured by the ZEUS collaboration.

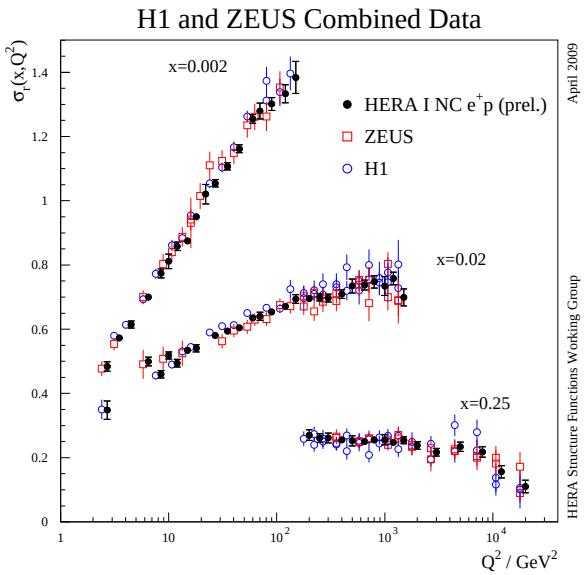

Fig. 3. The combined H1+ZEUS cross sections for NC DIS compared to measurements from the individual collaborations.

$$\tilde{\sigma}_{NC}^{e^\pm p} = F_2(x,Q^2) \mp \frac{Y_-}{Y_+} xF_3(x,Q^2) - \frac{y^2}{Y_+} F_L(x,Q^2) \qquad (2)$$

It can be seen that by measuring the reduced cross sections for e^+p and e^-p collisions and subtracting one from the other, it is possible to directly measure xF_3. The reduced cross sections for HERA-II e^-p data from a recent measurement by ZEUS [2] are shown in Fig. 1. together with data from a previous measurement of the reduced cross sections for e^+p data [3]. The predictions from the ZEUS-JETS next-to-leading-order(NLO)-QCD fit [4], which does not include the e^-p data, are also shown. It can be seen that $\tilde{\sigma}_{NC}^{e^-p}$ and $\tilde{\sigma}_{NC}^{e^+p}$ differ by more at larger values of Q^2. This corresponds to the SM expectation and occurs because the xF_3 contribution (dominated by interference between Z and γ exchange) becomes more significant at higher-energy scales. The reduced cross sections in Fig. 1. were used to extract the values of xF_3 shown in Fig. 2. This is the most precise direct measurement of xF_3 and agrees well with the predictions from the ZEUS-JETS QCD fit.

In addition to performing new measurements with HERA-II data, H1 and ZEUS have made considerable progress in the combination of results from HERA-I data [5]. In order to produce the combined results, the following strategy is adopted:

- all measurements are "swum" to a common x, Q^2 grid;
- the data are corrected to correspond to measurements at the same proton energy (920 GeV);
- the average cross sections and uncertainties for the points are calculated with a global combination, described in a recent H1 publication [6];
- the procedural uncertainties are calculated.

In total 1402 original points are combined into 741 points. The agreement of the H1 and ZEUS datasets can be quantified by the value of χ^2/n.d.f. for the combination. This is 637/656 indicating good agreement. There are 110 systematic uncertainties considered from the two experiments, and only 3 arising from the combination procedure. An example of the combined data compared to the individual measurements is shown in Fig. 3., it can be seen that the new combined measurements are much more precise than the measurements from the individual collaborations. The combined data attain a precision of 2% or better over a Q^2 range of $3 < Q^2 < 500\,\mathrm{GeV}^2$. Even more impressive precision of 1% or better is attained for $20 < Q^2 < 100\,\mathrm{GeV}^2$.

2.2. Measurements of F_L

From inspection of the expression for the reduced cross section in equation (2) it can be seen that only the xF_3 and F_L terms depend on all of Q^2, x and y whereas F_2 depends only on Q^2 and x. It is therefore possible to directly extract F_L by measuring the reduced cross section at different values of y for the same x and Q^2. This necessitates a change of centre of mass energy, $\sqrt{s}$ because, at any given s, Q^2 and x determine y via the relation $Q^2 = sxy$. To enable the first direct measurements of F_L, HERA dedicated several months of running time at lower proton energies of 460 GeV and 575 GeV. The first measurements from H1 [7] and ZEUS [8] have now been performed covering the kinematic region $12 < Q^2 < 90\,\mathrm{GeV}^2$ and $20 < Q^2 < 130\,\mathrm{GeV}^2$ respectively. The preliminary results of an attempt by H1 to extend the kinematic region to $5 < Q^2 < 800\,\mathrm{GeV}^2$ is shown in Fig. 4. The higher Q^2 measurements have much larger uncertainties, dominated by the statistical uncertainty. At lower Q^2 the precision is sufficient to distinguish between theoretical expectations for F_L.

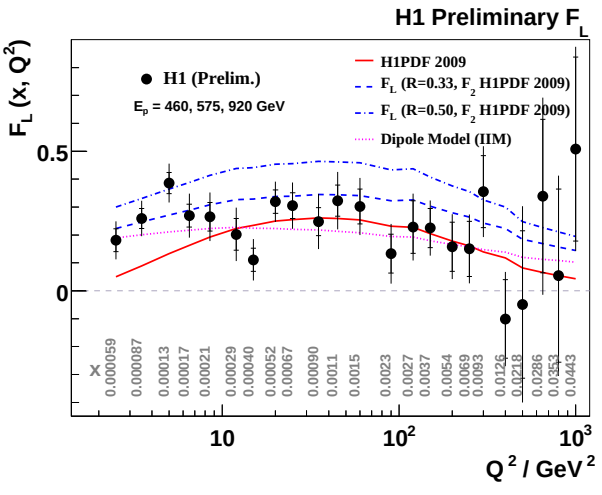

Fig. 4. The longitudinal structure function F_L measured by H1.

2.3. *Charged current cross sections*

The double differential cross section for charged current (CC) DIS can be written as [1]:

$$\frac{\mathrm{d}^2\sigma^{e^\pm p}_{CC}}{\mathrm{d}x\mathrm{d}Q^2} = \frac{G_F^2 M_W^2}{4\pi x(Q^2+M_W^2)^2}[F_2^{CC}(x,Q^2) - \frac{y^2}{Y_+}F_L^{CC}(x,Q^2) \mp \frac{Y_-}{Y_+}xF_3^{CC}(x,Q^2)]\,(1+\delta_r), \quad (3)$$

where M_W is the mass of the W boson and the structure functions F_i^{CC} are the structure functions for CC scattering. As with the NC cross section, the propagator $\frac{G_F^2 M_W^2}{4\pi x(Q^2+M_W^2)^2}$ and radiative correction can be divided out to give the reduced cross section $\tilde{\sigma}^{CC}_{e^\pm}$. For CC the reduced cross section is proportional (at leading order in QCD) to quark PDFs:

$$\tilde{\sigma}^{CC}_{e^+} \propto x[(1-y)^2(d+s)+\bar{u}+\bar{c}]$$
$$\tilde{\sigma}^{CC}_{e^-} \propto x[(1-y)^2(\bar{d}+\bar{s})+u+c].$$

Here, u, d, s, c are the relevant quark PDFs (functions of x and Q^2). This means that measurements of e^+p (e^-p) scattering cross sections provide information about the d-(u-)quark PDF. Thus CC cross sections provide complementary information about the PDFs to NC cross sections; the NC cross sections are dominated by the u-quark contribution for both beam charges.

Data from the latest preliminary measurement of $\tilde{\sigma}^{CC}_{e^+}$ from the ZEUS collaboration [9] are shown in Fig. 5. They are compared with predictions from the ZEUS-JETS QCD fit, which does not include these data. It can be seen, particularly at high values of Q^2 and x, that the uncertainties on the new ZEUS measurement are comparable to the uncertainty on the ZEUS-JETS prediction. Hence this data will be useful in constraining the d and s PDFs at higher Q^2 and x.

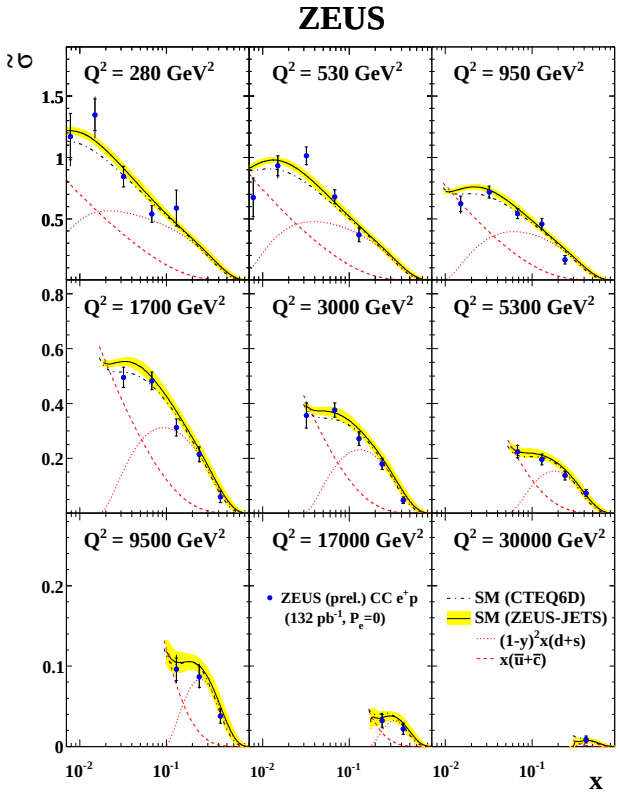

Fig. 5. The reduced cross section for CC DIS in e^+p scattering measured by ZEUS.

2.4. *QCD Fits*

Both H1 [10] and ZEUS [4] have performed NLO QCD fits to determine the PDFs of the proton using their data. The latest H1 result is typical of the approach used. Parametrisations of the following components of the proton are fitted : the up and down valence quarks xu_v and xd_v; the gluon xg, the up-type sea contribution $x\bar{U} = \bar{u} + \bar{c}$ and the down-type sea contribution $x\bar{D} = \bar{d} + \bar{s}$. The parametrisations are determined at a chosen value of Q^2, $Q_0^2 = 1.9\,\mathrm{GeV}^2$. The parametrised PDFs can then be evolved to different Q^2 using the DGLAP equations [11]. In these fits, heavy-flavour production is treated according to the general mass variable flavour numbering scheme of Thorne and Roberts [12]. The fit uses only H1 data from NC and CC scattering in the HERA-I running period. A good fit to the data is obtained with $\chi^2/\mathrm{n.d.f} = 587/644$.

The PDF uncertainties are reduced at low-x, compared to the previous H1 fit [13] (H1PDF2000). The PDF The uncertainties at higher-x are, however, larger than H1PDF2000. These larger uncertainties are more realistic: the increase comes from a new parametrisation uncertainty. The parametrisation uncertainty is determined by using parametrisations which describe the data well but have unphysical behaviour at high x.

A similar fitting procedure has been adopted to produce a fit to the combined H1+ZEUS data [5]. This new fit (HERAPDF0.2) is compared to data from NC scattering in Fig. 7.. It can be seen that the HERAPDF0.2 gives a very good fit to the data, the χ^2/n.d.f for the fit is 576/592. The precision of the new HERAPDF0.2 is comparable to the global fits from the CTEQ [14] and MSTW [15] groups. The fit gives much more precisely determined PDFs using the combined data than using

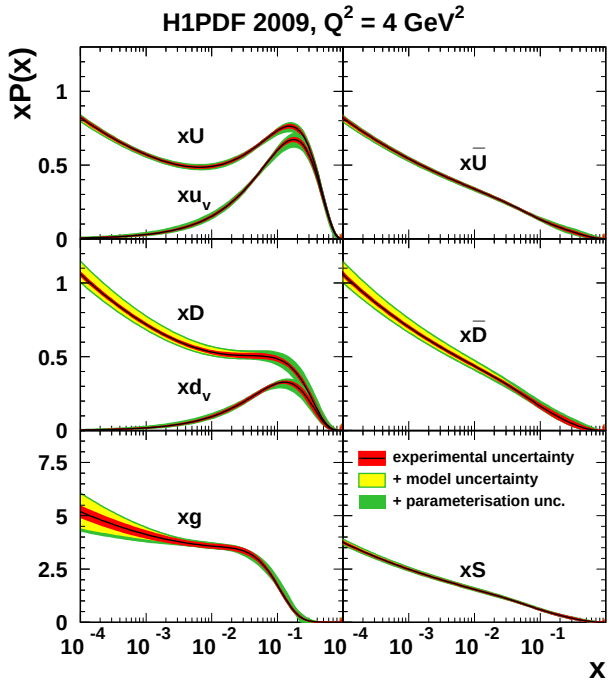

Fig. 6. The PDFs from the H1 PDF fit at $Q^2 = 4\,\mathrm{GeV}$.

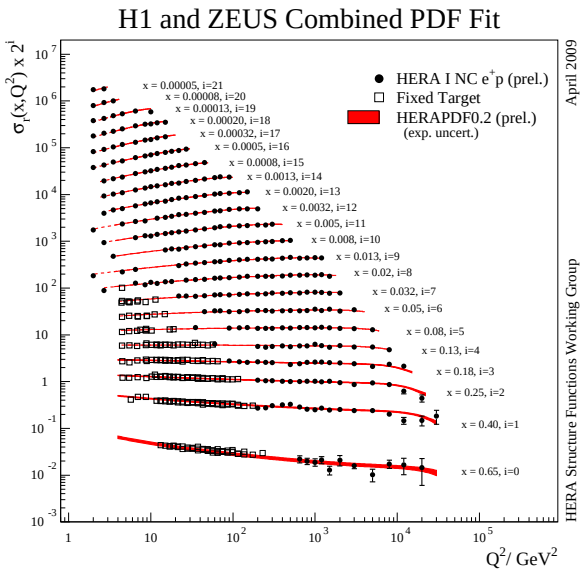

Fig. 7. Results from the H1+ZEUS combined PDF fit compared to HERA-I NC data.

the same H1 and ZEUS data separately.

The QCD fits discussed so far were performed using only HERA-I data sets. The HERA-II data sets include an order of

2.5. Heavy Flavour Production

Measurements of heavy-flavour production at HERA have not yet been included in the QCD fits performed by H1 and ZEUS. Addition of this data could add further sensitivity to the gluon distribution. This arises because the main production mechanism for heavy flavour production at HERA is boson-gluon fusion (BGF) where a γ and gluon produce a $Q\bar{Q}$ pair (where Q is a heavy quark) as show in Fig. 8. At HERA, these heavy flavour events can be tagged in three different ways:

- using heavy flavour-mesons such as the D^*;
- using leptons produced in semi-leptonic decays of the heavy quark;
- using inclusive impact parameter information.

These different tagging methods provide complementary measurements of heavy flavour production in DIS. They can be directly compared by extrapolating them to the charm structure function $F_2^{c\bar{c}}$ or beauty structure function $F_2^{b\bar{b}}$. In this section two new measurements of $F_2^{c\bar{c}}$ and $F_2^{b\bar{b}}$ are discussed: one from ZEUS[17] using semileptonic decays and one from H1[18] using inclusive impact parameter distributions.

The new ZEUS result includes the first measurement of $F_2^{c\bar{c}}$ using semileptonic decays into muons at HERA. A sample of DIS events with a muon and associated jet, in the kinematic region $Q^2 > 20\,\mathrm{GeV}^2$, was used. The fractions of such events arising from charm and beauty events were simultaneously extracted from a fit to three distributions that distinguish charm and beauty events from each other and from light quark events. These

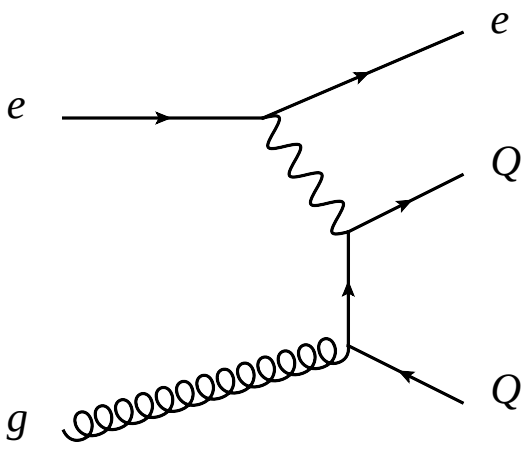

Fig. 8. Production of a heavy flavour quark antiquark pair in DIS via Boson-Gluon Fusion.

variables were: the muon momentum transverse to the axis of the associated jet, the impact parameter of the muon in the transverse plane and the missing transverse momentum parallel to the muon direction. The results were found to agree well with the NLO QCD predictions [19] and also well with previous measurements that were based on independent techniques.

The new H1 result makes use of inclusive impact parameter distributions to simultaneously fit the charm and beauty contributions to the DIS scattering cross section. The Q^2 range $5 < Q^2 < 2000\,\mathrm{GeV}^2$ is covered. Although the background from light flavour events is larger than in other methods, a larger region of the phase space for heavy quark induced events is used with this method. This means that the extrapolation from the measured cross sections to $F_2^{Q\bar{Q}}$ is smaller. The measurements agree well with the NLO QCD predictions.

A summary of $F_2^{c\bar{c}}$ measurements from H1 and ZEUS is shown in Fig. 9. Measurements using all three heavy flavour tagging methods are shown. It can be seen that a

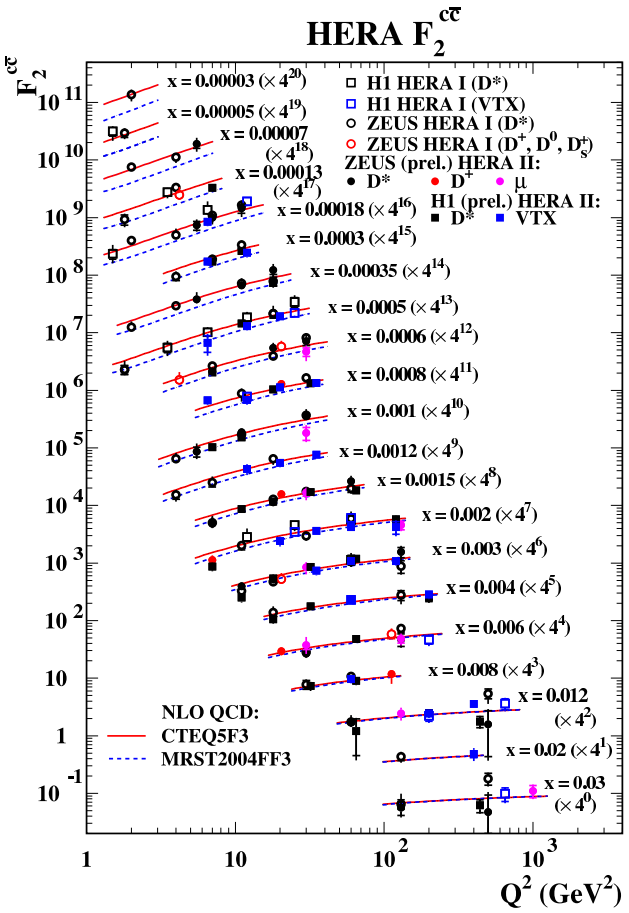

Fig. 9. HERA measurements of $F_2^{c\bar{c}}$.

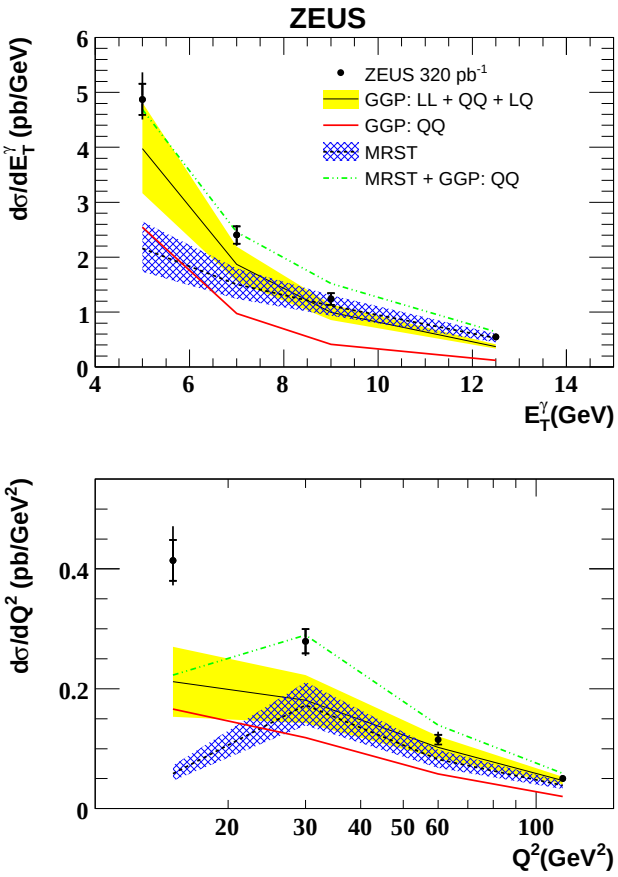

Fig. 10. Differential cross sections for isolated photon production in DIS from the ZEUS collaboration.

detailed and consistent picture of $F_2^{c\bar{c}}$ has been revealed by HERA. There is much smaller coverage of $F_2^{b\bar{b}}$, but more measurements are still expected from both H1 and from ZEUS. Inclusion of these measurements in QCD fits of the PDFs would provide, at the very least, an important consistency check for the gluon distribution. Combination of the H1 and ZEUS measurements is currently underway, and strong improvements in precision are expected.

2.6. Isolated γ Production

Isolated photons can be produced in DIS via photon radiation from the lepton or from a quark. The contributions to the cross section from lepton radiation (LL), quark radiation (QQ) and the interference (LQ) between them have been calculated at leading order in Quantum electrodynamics (QED) and QCD by Gehrmann-De Ridder *et al.* [20] (GGP). However, Martin *et al.* (MRST) have shown that an enhancement of the LL contribution would arise as a consequence of adding QED corrections to PDFs [21]. In this case the proton gains a photonic component (γ_P) which then undergoes Compton scattering $e\gamma_P \to e\gamma^*$. The measurement of this cross section is hence sensitive to the photonic component of the proton.

A new measurement of isolated photon production in DIS from the ZEUS experiment [22] in the kinematic range $10 < Q^2 < 350\,\text{GeV}$ has been made. The measured differential cross sections as functions of the photon transverse momentum, E_T^γ ($d\sigma/dE_T^\gamma$) and Q^2 ($d\sigma/dQ^2$) are compared to the theoretical calculations in Fig. 10. Since the MRST calculation does not include the QQ part of the cross section an hybrid calculation can be made by summing it with the QQ part of the GGP calculation (the LQ term can be neglected). It can be seen that the shape of the $d\sigma/dE_T^\gamma$ is well described both by GGP and the hybrid calculation (labelled MRST + GGP:QQ). However the GGP calculation significantly underestimates the differential cross section at low Q^2, as was also observed in a recent measurement by H1 [23]. The hybrid calculation improves the description of $d\sigma/dQ^2$, but still underestimates the differential cross section at lowest Q^2. A version of the MSTW08 PDFs [15] incorporating QED corrections is under preparation and may offer an improvement in description of the data.

3. Jets

Jet measurements at HERA are a precision test of QCD. The measured cross sections depend on the gluon content of the proton and on the magnitude of the strong coupling. Statistical precision is typically very good and, experimentally, the usual limitation on precision comes from the jet-energy-scale uncertainty. In this section recent results from jet measurements in high-Q^2 DIS are reviewed.

*This photonic component of the proton would have consequences for calculations of electroweak corrections to cross sections at the LHC and TeVatron.

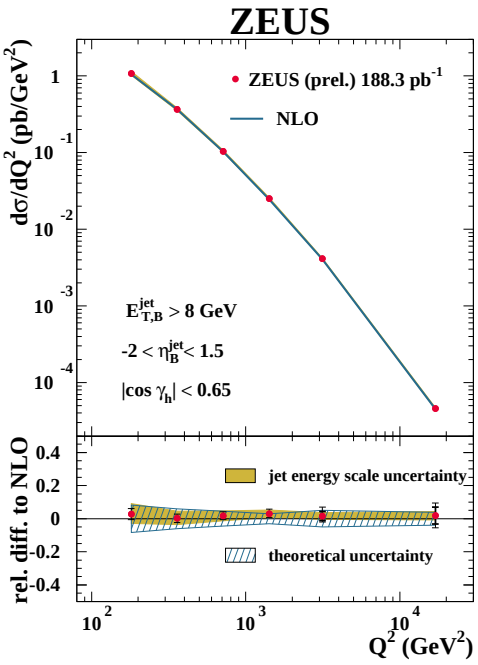

Fig. 11. The differential cross section for inclusive jet production in high-Q^2 DIS, measured by the ZEUS collaboration.

3.1. Jet production in DIS

The ZEUS collaboration have recently measured the cross sections for inclusive jet production in DIS at high-Q^2 ($Q^2 > 125\,\mathrm{GeV}^2$) [24]. The analysis uses a sample of NC DIS events containing at least one jet with E_T in the Breit frame [1] greater than 8 GeV and pseudorapidity in the Breit frame within the region $-2 < \eta^{\mathrm{jet}} < 1.5$. The measured differential cross section as a function of Q^2 is compared to NLO QCD predictions from the programme DISENT [25] in Fig. 11. It can be clearly seen that the measurements agree well with the predictions. It can also be seen that the precision of the measurement is often better than that of the predictions. In the regions where this is true, the uncertainty on the prediction is often dominated by the uncertainty on the gluon PDF, thus this measurement can constrain the gluon PDF if used as an input to a PDF fit.

The H1 collaboration has also recently presented a new measurement of inclusive jet production in high-Q^2 DIS ($150 < Q^2 < 15000\,\mathrm{GeV}^2$). This measurement is presented alongside a measurement of the normalised cross sections (e.g. the ratios to the fully inclusive NC cross section) for two- and three-jet production. The normalised dijet cross section is compared to predictions from DISENT and NLOJET++ [26] in Fig. 12. The comparison is shown as a function of ξ, the momentum fraction carried by the incoming parton:

$$\xi = x(1 + \frac{M_{12}}{Q^2}),$$

where M_{12} is the dijet invariant mass. It is clear that the H1 measurements are significantly more precise than the predictions over a large part of the kinematic range. In this case the dominant uncertainties on the predictions come from missing higher order terms for the calculation.

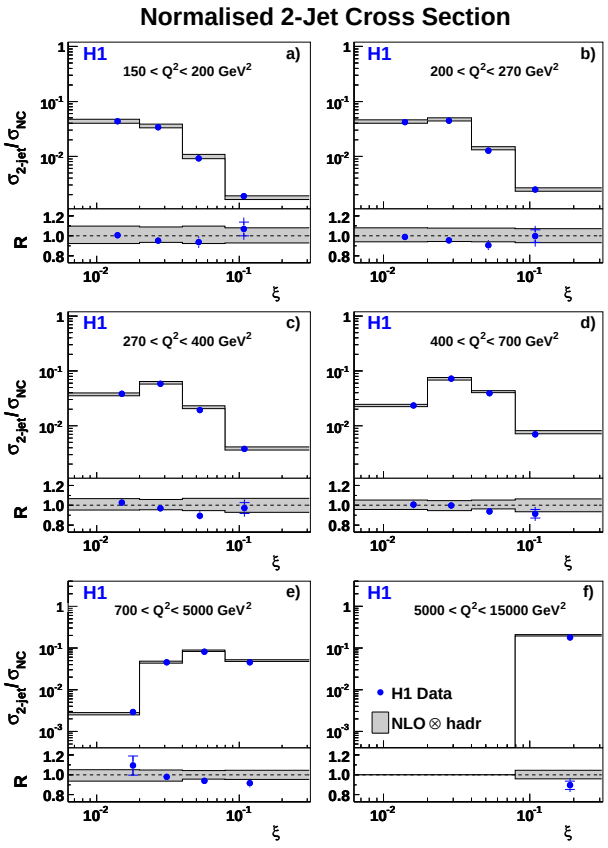

Fig. 12. The normalised cross section for dijet production in High-Q^2 DIS, measured by the H1 collaboration.

3.2. Measurements of the strong coupling

Jet cross-section measurements at HERA are sufficiently precise to enable measurement of the strong coupling α_S. This is done by performing the theoretical calculation using different values of α_S (and appropriate PDF sets) in order to make a phenomenological parametrisation of the cross section as a function of α_S. This establishes a direct mapping from a measured cross section to α_S with associated uncertainty. A summary plot of selected measurements of α_S, including those described in section 3.1., is shown in Fig 13. The H1 measurement at high Q^2 is of comparable experimental precision to the measurement from four-jet events at LEP and to the world average [27]. The impressive success of QCD is visible, with consistent measurements from differing environments and energy regimes.

3.3. Jet Substructure

The study of the substructure of jets can provide information about the pattern of radiation from the primary parton initiating the jet. In ep collisions, substructure can also be used to explore colour coherence by studying to what extent the soft radiation is emitted in the direction of the proton. Jet substructure is usually studied by defining jets using a certain algorithm e.g the k_T algorithm [28], and then running a different algorithm (or the same algorithm with different parameters) on the constituents of the jets found by the original algorithm. Recently jet substructure has been suggested as a useful tool for searching for boosted heavy particles at the LHC [29]. Any such usage will be contingent on the substructure of jets from background QCD processes being

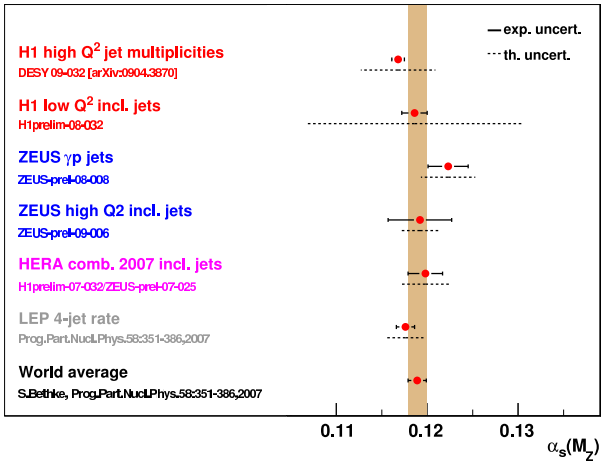

Fig. 13. A summary of α_S measurements from HERA.

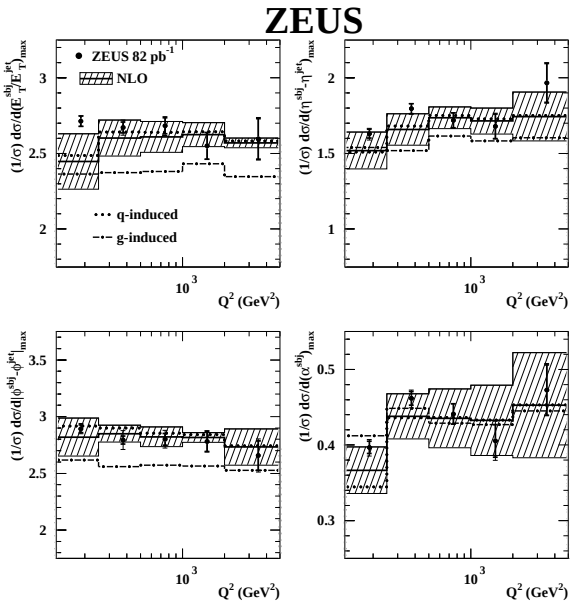

Fig. 14. Maxima of the normalised two-subjet differential cross sections as a function of Q^2 compared to QCD calculations. for comparison, NLO predictions for gluon and quark indiced jets are also shown separately.

well understood.

The ZEUS collaboration has recently produced two new substructure measurements, one of jets with exactly two subjets [30] and one of jets with exactly three subjets [31]. In both cases jets are first selected by running the k_T algorithm in the longitudinally invariant inclusive mode. The subjet analysis is made by running the exclusive k_T algorithm on the constituents of these jets using a resolution parameter $y_{\rm cut}$ of 0.05 (the two subjets measurement) or 0.03 (the three subjets measurement). The measurement kinematic region $Q^2 > 125\,\mathrm{GeV}^2$ was used for both measurements. The measured normalised subjet cross sections for the two-subjet analysis as a function of Q^2 are compared to predictions from DISENT in Fig 14.. The results agree adequately with the perturbative QCD predictions over a large range of Q^2. the precision of the data is often better than that of the predictions. The measurements of jets with three-subjets leads to similar conclusions. The capability of pQCD to describe QCD jet substructure is encouraging for application of such infromation in new physics searches.

4. Summary

With data taking complete, the HERA experiments continue to produce important QCD measurements. HERA produces world leading PDF measurements: the newest data at high Q^2 will help to further constrain quark PDFs, while jet and heavy flavour messages yield important information about the gluon density. Isolated photon events in DIS also offer the opportunity to probe the photonic component of the proton. Jet production at HERA is a rich testing ground for QCD, extremely precise measurements of the strong coupling have been made and the precision of jet cross sections is often limited by theoretical input. As attention at the LHC turns to jet substructure as a tool for new physics searches, measurements of these quantitities at HERA can help us to assess our understanding of this aspect of QCD. Not content with these separate precise QCD measurements, the H1 and ZEUS collaborations have worked together to produce a combination technique for their data that provide structure function measurements of unsurpassed precision.

References

[1] R. Devenish and A. Cooper-Sarkar *Deep inelastic scattering* (2004) Oxford Univ. Pr., Oxford, UK.
[2] ZEUS Coll., S. Chekanov *et al.*, Eur. Phys. J. C62 (2009) 625
[3] ZEUS Coll., S. Chekanov *et al.*, Phys. Rev. D70 (2004) 052001
[4] ZEUS Coll., S. Chekanov *et al.*, Eur. Phys .J. C42 (2005) 1
[5] H1 Coll., H1-Prelim-09-045, ZEUS Coll., ZEUS-Prel-09-011, available from: http://www-h1.desy.de/h1/www/publications/htmlsplit/H1preli
[6] H1 Coll., F.D. Aaron *et al.* arXiv:0904.0929 [hep-ex] Accepted by Eur. Phys J. C.
[7] H1 Coll., F.D. Aaron *et al.* Phys. Lett. B665 (2008) 139
[8] ZEUS Coll., S. Chekanov *et al.* arXiv:0904.1092 [hep-ex]
[9] ZEUS Coll., S. Chekanov *et al.*, ZEUS-Prel-09-002, available from: http://www-zeus.desy.de/public_results/functiondb.php?id=ZEU
[10] H1 Coll., F.D. Aaron *et al.* arXiv:0904.3513 [hep-ex] Accepted by Eur. Phys J. C.
[11] V.N. Gribov, L.N. Lipatov, Sov. J. Nucl. Phys. 15 (1972) 438
V.N. Gribov, L.N. Lipatov, Sov. J. Nucl. Phys. 15 (1972) 675
L.N. Lipatov, Sov. J. Nucl. Phys. 20 (1975) 94
G. Altarelli and G. Parisi, Nucl. Phys. B126 (1977) 298.
Yuri L. Dokshitzer, Sov. Phys. JETP 46 (1977) 641.
[12] R.G. Roberts and R.S. Thorne, Phys. Rev. D57 (1998) 6871.
[13] H1 Coll., C. Adloff *et al.*. Eur. Phys. J. C30 (2003) 1.
[14] P. M. Nadolsky *et al.*, Phys. Rev. D78 (2008) 013004.
[15] A.D. Martin *et al.*. Eur. Phys. J C63 (2009) 189.
[16] ZEUS Coll., S. Chekanov *et al.*, ZEUS-Prel-09-010, available from: http://www-zeus.desy.de/public_results/functiondb.php?id=ZEU
[17] ZEUS Coll., S. Chekanov *et al.* arXiv:0904.3487 [hep-ex]
[18] H1 Coll., F.D. Aaron *et al.* arXiv:0907.2643 [hep-ex]
[19] B.W. Harris and J. Smith, Nucl. Phys. B452

(1995) 109.
B.W. Harris and J. Smith, Phys. Lett. B353 (1995) 109. Erratum-ibid. B359 (1995) 423
[20] A. Gehrmann-De Ridder *et al.*. Phys. Rev. Lett. 96 (2006) 132002.
[21] A.D. Martin *et al.*. Eur. Phy. J. C39 (2005) 155.
[22] ZEUS Coll., S. Chekanov *et al.*, arXiv:0909.4223 [hep-ex].
[23] H1 Coll., F.D. Aaron *et al.* Eur. Phys. J. C54 (2008) 371.
[24] ZEUS Coll., S. Chekanov *et al.*, ZEUS-Prel-09-006, available from: http://www-zeus.desy.de/public_results/functiondb.php?id=ZEUS-prel-09-006
[25] S. Catani and M.H. Seymour, Nucl. Phys. B485 (1997) 291. Erratum-ibid. B510 (1998) 503
[26] Z. Nagy and Z. Trocsanyi, Phys. Rev. Lett 87 (2001) 082001
[27] S. Bethke, Prog. Part. Nucl. Phys. 58 (2007) 351
[28] S.D. Ellis and D.E. Soper, Phys. Rev. D48 (1993) 360.
S. Catani *et al.*, Nucl. Phys. B406 (1993) 187.

[29] M. H. Seymour, Z. Phys. C62, (1994) 127.
J. M. Butterworth *et al.*, Phys. Rev. D65, (2002) 096014.
J. M. Butterworth *et al.*, Phys. Rev. Lett. 100, (2008) 242001.
D. E. Kaplan *et al.*, Phys. Rev. Lett. **101**, (2008) 142001.
J. Thaler and L.-T. Wang, JHEP **07**, (2008) 092 .
S. D. Ellis *et al.*, arXiv:0903.5081 [hep-ph].
L. G. Almeida *et al.*, Phys. Rev. **D79**, (2009) 074017 .
[30] ZEUS Coll., S. Chekanov *et al.*, arXiv:0812.2864 [hep-ex].

[31] ZEUS Coll., S. Chekanov *et al.*, ZEUS-Prel-09-007, available from: http://www-zeus.desy.de/public_results/functiondb.php?id=ZEUS-prel-09-007